In vivo 3-dimensional Magnetic Resonance Wall Shear Stress Estimation in Ascending Aortic Dilatation

Erik T. Bieging[1], **Alex Frydrychowicz**[1], **Andrew Wentland**[2], **Benjamin R. Landgraf**[1], **Kevin M. Johnson**[2], **Oliver Wieben**[1,2], and **Christopher J. François**[1]

[1] Department of Radiology, University of Wisconsin – Madison

[2] Department of Medical Physics, University of Wisconsin – Madison

Abstract

Purpose—To estimate surface-based wall shear stress (WSS) and evaluate flow patterns in ascending aortic dilatation (AscAD) using a high-resolution, time-resolved, three-dimensional (3D), three-directional velocity encoded, radially undersampled phase contrast magnetic resonance sequence (4D PC-MRI).

Materials and Methods—4D PC-MRI was performed in 11 patients with AscAD (46.3±22.0 years) and 10 healthy volunteers (32.9±13.4 years) after written informed consent and IRB-approval. Following manual vessel wall segmentation of the ascending aorta (MATLAB, The Mathworks, Natick, MA), a 3D surface was created using spline interpolation. Spatial WSS variation based on surface division in 12 segments and temporal variation were evaluated in AscAD and normal aortas. Visual analysis of flow patterns was performed based on streamlines and particle traces using EnSight (v9.0, CEI, Apex, NC).

Results—AscAD was associated with significantly increased diastolic WSS, decreased systolic to diastolic WSS ratio, and delayed onset of peak WSS (all *P* < 0.001). Temporally averaged WSS was increased and peak systolic WSS was decreased. The maximum WSS in AscAD was on the anterior wall of the ascending aorta. Vortical flow with highest velocities along the anterior wall and increased helical flow during diastole were observed in AscAD compared to controls.

Conclusion—Changes in WSS in the ascending aorta of AscAD correspond to observed alterations in flow patterns compared to controls.

Keywords

flow-sensitive MRI; ascending aortic aneurysm; wall shear stress; hemodynamics

Introduction

The incidence of ascending aortic aneurysm (AscAA) diagnosis is rising, likely due to increased use of noninvasive diagnostic imaging (1). Empirically, aortic aneurysms are seen with higher frequency in patients with Marfan Syndrome, Ehlers-Danlos Syndrome, and bicuspid aortic valve (1-2). However, the precise mechanisms of AscAA formation are not yet completely understood.

AscAA have an increased risk of dissection, rupture, or death, approximately 5 to 15% per year depending on aorta diameter (3), which emphasizes the need for early detection and

Corresponding Author: Christopher J. François, Assistant Professor, Department of Radiology, University of Wisconsin – Madison, E1/Clinical Science Center, 600 Highland Avenue, Madison, WI 53792-3252, cfrancois@uwhealth.org, 608-263-1198.

close follow-up. Currently, the probability of rupture is estimated solely on the basis of aneurysm diameter and change in diameter over time (3) which are taken into consideration when deciding when to perform AscAA repair. The ability to analyze the hemodynamic forces and biomechanical properties of the vessel wall that potentially contribute to aneurysm growth and rupture could be useful in determining the appropriate time for intervention.

The extent to which hemodynamic patterns influence aneurysm formation and/or development is an active area of debate. As the largest artery and most immediate recipient of blood from the left ventricle, the ascending aorta accommodates characteristically complex flow with each heartbeat. Alterations in flow patterns are observed in AscAA (4-5) and may induce altered dynamic shear stresses upon the vessel wall. Alterations in wall shear stress (WSS) have previously been shown to be associated with atherosclerosis formation and plaque stability (6-7). Although controversial, changes in WSS have also been implicated in the development and growth of aneurysms – with high WSS associated with initiation (8) and low WSS correlated with growth of (9) cerebral aneurysms.

Previous studies using *in vitro* models and computer aided analyses using computational fluid dynamics (CFD) have shown promising results based on true patient anatomic models and inflow conditions (10-11). Using patient specific ascending aorta models, Jin, *et al.* calculated relatively consistent WSS values around the circumference of the aorta (10). While there are no CFD WSS studies in true patient AscAA models, studies in abdominal aortic aneurysms have shown decreased intra-aneurysmal WSS (12-14).

Recently, 3D phase contrast magnetic resonance imaging (PC MRI) has been used to estimate WSS *in vivo* (8,15-22). 3D PC MRI, with 3D flow velocity data and high spatial resolution, can be used to characterize 3D flow patterns. Several studies have used this method to estimate WSS in the ascending aorta (15,17-19). In healthy volunteers, Frydrychowicz, *et al.* observed time averaged WSS to be greatest on the inner and outer curvature of the ascending aorta, and lowest on the left and right walls (19). While WSS magnitude does vary around the circumference of the aorta in healthy subjects, variations were more pronounced in patients with a variety of cardiovascular disease. For example, WSS was increased along the anterior wall of the ascending aorta in aortic valve stenosis (18) and altered WSS values were present in descending thoracic aortic aneurysm as well (17). These studies demonstrate that visibly pathologic flow patterns can lead to measureable alterations in WSS. Barker, *et al.* (15) found asymmetric WSS values around the circumference of the ascending aorta in patients with bicuspid aortic valves (BAV). These results provide evidence to suggest a relationship between WSS changes and AscAA formation in patients with BAV.

Limitations of current 3D PC MRI techniques include the relatively low spatial resolution, which contributes to systematic underestimations of WSS (21), and relatively lengthy acquisition times. For our study, we used a 3D radially undersampled (Vastly undersampled Isotropic Projection Reconstruction, VIPR) PC MRI technique (23-24) to acquire isotropic, high spatial resolution PC data in reduced imaging times. While the resolution of the technique we used for our study may be far from the resolution necessary to measure the true WSS, increased spatial resolution should, theoretically, improve WSS estimation. The purpose of this study was to use the isotropic, high spatial resolution, 3D data to (A) estimate WSS over a 3D vessel surface of the ascending aorta, rather than at specific cutplanes (15,19,22), (B) to calculate the spatial and temporal WSS differences in patients with ascending aortic dilation (AscAD), and (C) to see how these findings are related to alterations in flow patterns of AscAD.

Materials and Methods

MRI Acquisition

This HIPAA-compliant, prospective study was approved by our Health Sciences Institutional Review Board and written informed consent was obtained from all subjects prior to inclusion in the study.

MRI studies were performed in 11 subjects (7 men, 4 women, ages 10 – 85 years, mean age: 46.3 ± 22.0 years) with known AscAD, and in 10 normal healthy volunteers (6 men, 4 women, ages 21 – 54 years, mean age: 32.9 ± 13.4 years). Maximum diameter of the ascending aorta was 43.7 ± 5.3 mm in AscAD and 31.3 ± 3.0 mm in controls. Height and weight, which were used to determine body surface area (BSA) and subsequently aortic size z-scores (25) and aortic size indices (26), were available in 8/11 AscAD subjects. The mean ascending aorta z-score was 6.12 ± 1.34 (range: 4.38-7.41) and the mean aortic size index was 2.43 ± 0.39 cm/m^2 (range: 1.90-2.91). In 7/8 of the subjects for which we had information on BSA, the mean ascending aorta diameter was more than two standard deviations greater than the mean based age and BSA reported by Wolak, *et al* (27). BAV was present in 7/11 AscAD and in none of the controls. None of the subjects with AscAD had Marfan or Ehlers-Danlos Syndrome.

Studies in patients were performed on 1.5T (HDx) and 3.0T (HDx and MR750) scanners (GE Healthcare) while studies in normal volunteers were all performed at 3.0T (MR750, GE Healthcare). Following intravenous contrast administration (0.1mmol/kg gadobenate dimeglumine, MultiHance, Bracco Diagnostics, Inc., Princeton, NJ), PC data was acquired using a 4-point PC VIPR sequence (24,28-29) with an 8-channel body (1 patient) or cardiac (10 patients, 10 volunteers) coil. PC VIPR was performed after the administration of intravenous contrast to maximize the intravascular signal-to-noise ratio (30). Parameters for the PC VIPR sequence were adapted to the individual subject's anatomy: imaging volume = 260 - 360 mm^3 isotropic; TR = 6.4 – 11.9 ms; TE = 2.1 – 3.9 ms; 1.0 - 1.4 mm^3 isotropic spatial resolution; VENC = 80 cm/s (10 volunteers, 9 patients), 150 cm/s (1 patient) or 350 cm/s (1 patient); scan time of approximately 10 minutes. The PC VIPR volume was aligned such that the acquisition extended from above the aortic arch to level of the diaphragm. Respiratory gating was performed with an adaptive gating scheme based on bellows readings and 50% respiratory gating efficiency. Data were reconstructed into 20 time frames over the cardiac cycle using retrospective ECG-gating. Images were reconstructed using a tornado filter (31) so that the update rate at the center of k-space was one twentieth of one R-R interval, giving a reconstructed temporal resolution of 1/20th of the R-R interval.

Vessel Segmentation and WSS Estimation

Vessel surfaces were manually segmented (Figure 1) and WSS was estimated and analyzed using home-built software (MATLAB, The Mathworks, Natick, MA). To account for motion of the aorta, surfaces were defined at each time frame during systole. A single surface was defined and used for all diastolic frames because of the lower velocity-noise ratio during diastole. Vessel walls were defined in axial cutplanes at intervals of no greater than 5 voxels ranging from the aortic annulus up to the bottom of the aortic arch. User defined vessel wall points were selected on each axial cutplane complex difference image to create closed-loop cubic splines around the ascending aorta vessel boundary. The centroid of each closed-loop axial spline was automatically determined. A set number of points on the spline were interpolated to define the vessel boundary in the cutplane, forming evenly spaced angles with the centroid (Figure 1A). The number of points (80 – 170) was the maximal circumference of the vessel plus an oversampling factor of approximately 10% in order to ensure usage of all available flow data. Longitudinal cubic splines were computed

between points in adjacent cutplanes along each radial position around the vessel. A set of surface points was determined by interpolation of the longitudinal splines at a user-defined number of points (50 – 100). This number was the length of the defined vessel plus an oversampling factor of approximately 10%.

A unit inward surface normal vector was determined for each surface point from the derivatives of both the axial and vertical splines. The velocity vector field was determined from the PC VIPR data. For each surface point, three velocity vectors were computed by 3D linear interpolation of the acquired data from the following points: the vessel wall, one unit distance inward from the wall, and two unit distances inward from the wall. The cross product of each velocity vector and the surface inward unit normal vector were taken to obtain the velocity component tangent to the vessel surface. WSS was calculated based on the following equation:

$$WSS = \mu \frac{\partial v}{\partial n} \quad \text{[Equation 1]}$$

where μ is the viscosity of fluid, v is the three dimensional velocity vector, and n is the wall normal vector (Figure 1B). The linear least squares method was applied to these three velocity vectors and used estimate the derivative of the tangential velocity at the vessel wall. Blood was assumed to be a Newtonian fluid with a viscosity of 4.0 cP. The WSS magnitude was then estimated by multiplying by this assumed viscosity constant.

WSS Analysis

In order to evaluate spatial differences in WSS, the ascending aorta was divided into 4 circumferential segments and 3 axial segments, for a total of 12 segments (Figure 1). Circumferential segmentation was performed by dividing the vessel into 4 equal quadrants based on angle from the vessel centroid. Divisions were defined such that the segment boundaries delineated the walls of the aorta's anterior outer curvature, posterior inner curvature, and right and left sides (anterior, posterior, left and right). Axial segmentation was performed by dividing the vessel into 3 equal segments (proximal, middle, and distal). Because of the curvature of the aorta, the vessel surface area represented by each surface point was variable. Therefore, average WSS on each segment was taken as an area-weighted average of WSS. This average WSS was determined for each time frame to obtain functions of WSS over time on each segment.

Five parameters were extracted from each WSS function: time averaged WSS, peak WSS, time to peak WSS, diastolic baseline WSS, and percent increase of WSS from baseline to peak. Time averaged WSS (WSS_{avg}) was the average WSS over all 20 time frames. Peak systolic WSS (WSS_s) was the maximum WSS over the cardiac cycle. Time to peak WSS (t_{max}) was the phase in the cardiac cycle at which was maximum. Diastolic baseline WSS was determined as the average of the last 5 time frames of the cardiac cycle. The peak systolic to diastolic WSS ratio (s/d_{WSS}) was the peak systolic (WSS_s) divided by the diastolic baseline WSS (WSS_d). This ratio was computed to quantify the relative change in WSS magnitude over the cardiac cycle. High s/d_{WSS} corresponds to large variation in WSS magnitude over the cardiac cycle while low s/d_{WSS} corresponds to a more constant baseline level of WSS.

Flow Visualization

Blood flow visualization was achieved using commercially available visualization software (*EnSight* 9.0, CEI, Apex, NC). For qualitative analysis, streamlines and temporally resolved particle traces were created based on the acquired 3D velocity fields. Data was visually

analyzed with color-coding for velocities with software allowing for a full temporal and spatial appreciation of the data. The following velocity patterns were evaluated: secondary flow characteristics (helical and/or vortical flow patterns) where helical flow was defined as rotational flow around the long axis of the vessel in an entirely anterograde direction. The presence of supra-physiologic helical flow was only noted if more than one full 360° rotation occurred within the ascending aorta, in order to exclude physiologic flow rotations known to occur in normal individuals. Vortical flow was defined as rotational flow around an axis transecting the vessel composed of both anterograde and retrograde components.

Statistical Analysis

Differences in WSS parameters (WSS_{avg}, WSS_s, t_{max}, s/d_{WSS}, WSS_d), over the entire aorta and for each segment, between AscAD and normal subjects were assessed using the unpaired Student t-test (two-tailed). Differences in WSS values between different segments were assessed using the paired Student t-test (two-tailed). Confidence intervals of 95% were used, values of $P < 0.05$ were accepted as statistically significant. To assess intra- and inter-observer variability, WSS analysis was repeated by two reviewers in eight subjects (four normal volunteers and four AscAD) more than six months after the initial analysis by the first reviewer. Variability was assessed using the method of Bland-Altman.

Results

WSS Analysis

Results of WSS calculations are summarized in Table 1. Although mean time-averaged WSS over the entire ascending aorta was higher in AscAD than in controls, the difference was not statistically significant ($P = 0.07$). Similarly, peak systolic WSS was lower in AscAD than in controls, but this difference was not statistically significant ($P = 0.17$). There was a statistically significant difference in diastolic WSS between patients with AscAD and controls ($P < 0.001$). The systolic to diastolic WSS ratio was significantly reduced in AscAD ($s/d_{WSS} = 3.57 \pm 1.06$) compared to controls ($s/d_{WSS} = 8.29 \pm 2.44$) ($P < 0.001$). Time to peak WSS occurred significantly later in the cardiac cycle in AscAD ($t_{max} = 6.1 \pm 1.0$) compared to controls ($t_{max} = 3.7 \pm 1.1$) ($P < 0.001$). When analyzed on a segment-by-segment basis, the diastolic WSS was significantly higher in AscAD on each of the 12 segments (all $P < 0.01$). Systolic to diastolic WSS ratio was significantly higher in AscAD on each segment (all $P < 0.05$). Time of peak WSS occurred significantly later in the cardiac cycle ($P < 0.05$) on all segments but one (proximal posterior).

In healthy controls, time averaged WSS values were increased on the anterior, right and distal segments and reduced on the left and proximal segments (all $P < 0.05$). In patients with AscAD, time averaged WSS was increased in the anterior and middle segments and was reduced in the right and proximal segments (all $P < 0.05$). In controls, peak systolic WSS was increased on the right side of the vessel. In AscAD, peak systolic WSS was increased on the anterior and middle segments, and was reduced on the posterior segment (all $P < 0.05$). Diastolic WSS in controls was increased on the posterior and distal segments, and was reduced on the right and middle segments (all $P < 0.05$).

Flow Visualization

Secondary flow characteristics were present in all AscAD patients and in 5 out of 10 controls (p<0.05). 5 controls showed non-rotational flow throughout systole and little flow during diastole (Figures 3B, 4B). Supra-physiologic helical flow occurred in all 11 AscAD patients, most commonly during diastole. Helical flow patterns were also noted in 4/10 control subjects. Vortical flow was noted in 8/11 AscAD patients and in 4/10 controls. The predominant flow pattern observed in AscAD was a high flow velocity along the anterior

wall of the aneurysm with a vertical vortex forming behind (Figure 3A). During late systole and early diastole, the vortex rotated horizontally and formed a right handed helix (Figure 4A). Helical flow persisted into diastole in all patients, and typically slowed as the phase progressed. Observed flow velocities during diastole were higher in AscAD.

Intra- and Inter-observer Variability

The results of the intra- and inter-observer variability analysis are summarized in Table 2. Intra-observer variability was lower than inter-observer variability. Variability was greater for peak systolic WSS measurements than for time-averaged and diastolic baseline WSS measurements. The variability was less than the difference in means between AscAD and controls in all parameters.

Discussion

In this study, time-resolved, 3D phase contrast MRI with radial undersampling (PC VIPR) was used to acquire 4D flow datasets in patients with AscAD and healthy volunteers. A spline based manual surface definition method was used to assess WSS *in vivo*. PC VIPR provided a better temporal and spatial resolution compared to previous *in vivo* flow analyses. As opposed to previously described Cartesian acquisition schemes, PC VIPR further allowed for effective scanning with large volume coverage and reasonable scan times. Further, a spline based manual surface definition method was successfully applied to assess WSS *in vivo* on the entire vessel wall, in contrast to approaches that extract 2D cutplanes from the acquired volumes thereby abandoning the fully 3-dimensional and 3-directional nature of such flow data. Results show that WSS values are in the same order as those reported previously (15,17-19).

Interestingly, our findings of increased WSS during diastole in AscAD correspond well with our observation of increased helical flow patterns during diastole in these patients, in concordance with previous studies demonstrating helical flow patterns in AscAD during systole (4,32) which may persist beyond systole and into diastole (33). While helical flow in the distal ascending aorta has been observed in normal volunteers (4,33-34), the presence of AscAD may support increased and sustained helicity which could account for the increased wall shear forces in these areas. Although it is not possible to determine without longitudinal data, these relatively elevated diastolic shear forces may contribute to aortic aneurysm growth.

Patients with AscAD also demonstrated delayed onset of peak systolic WSS compared to controls. This occurred in all segments of the ascending aorta. Since WSS and flow velocity are interrelated, this finding is congruent with results reported by Hope, *et al.* (4) in which they found a delay in peak flow velocity in AscAD. The delay in peak velocity and WSS can potentially be explained by the increased volume of the ascending aorta in AscAA and the dissipation of kinetic energy during systole as the increased volume of the ascending aorta is filled.

The vortical flow patterns and accelerated flow velocities along the anterior wall of the aorta in AscAA are also concordant with previous studies (4-5,34-36). Although vortical flow patterns have been reported to occur in normal volunteers in the sinuses of valsalva (34,37-38), they occur less frequently in the center of the ascending aorta (39). Vorticies in normal volunteers observed in this study were smaller and occurred less frequently than those observed in patients with AscAD. In AscAD, the highest systolic WSS was found along the anterior wall of the ascending aorta. High flow velocity along the anterior wall of the aneurysm, as reported previously (4-5) and observed in this study, induces increased shear stress in that location. Vortical flow, turbulent flow, and slower anterograde flow all

observed during systole along the posterior, left and right walls of the ascending aorta lead to lower WSS in these segments. This indicates the existence of significantly increased WSS gradients around the circumference of the aorta during peak systole in AscAD.

The ratio of peak systolic WSS to diastolic WSS was reduced in AscAD when compared to controls. The systolic to diastolic ratio can be interpreted as a measure of the pulsatility of WSS magnitude. AscAD had a more constant and less pulsitile pattern of WSS throughout the cardiac cycle, primarily due to an increase in the diastolic WSS in AscAD compared to controls. Although the lower peak systolic WSS values in AscAD were not statistically significant, this also contributes to the reduction in the systolic to diastolic WSS ratio. Hope, *et al.* suggested that helical flow may act to dampen oscillation between systolic and diastolic flow velocities (4). Slower onset of peak flow velocities combined with increased helical flow may act to dampen the pulsitility of WSS in AscAD.

While known to be a major influence on endothelial cell biology, accurate measurement of WSS *in vivo* has been elusive. Computational fluid dynamics (CFD) can be used to estimate WSS and achieves spatial resolutions far greater than those obtainable with purely MRI-based methods. However, CFD calculations are limited by assumptions made within each model. The WSS estimations made using PC MRI are typically lower than those reported in CFD studies (19). This is primarily due to the relatively low spatial resolution which leads to inaccurate measurement of flow velocities at the vessel wall. The mean WSS estimations in our study in normal ascending aortas are lower than those reported using CFD, but the temporal WSS patterns we observed are similar to those found using CFD (10). The WSS values we reported are on the same order as previous PC MRI studies using slightly lower spatial resolution. Although the accurate measurement of absolute WSS values may still not be obtainable with current 4D PC MRI techniques, their potential value and clinical importance may only require consistent relative estimates that can identify normal and abnormal WSS patterns *in vivo*.

A weakness of the WSS estimates in our study was the restriction to the magnitude of computed WSS vectors without investigation of information inherent in the detailed directionality. Although its value has not been proven so far, other studies have quantified circumferential properties of WSS, acknowledging that helical or vortical flow patterns may profoundly influence these properties (15,17-19). In addition, the temporal evolution of anterograde and retrograde WSS, which is only partially reflected in the systolic to diastolic WSS ratio, may be better appreciated in established parameters such as the oscillatory shear index (OSI) (7), which we did not evaluate in this study. While previous studies computed WSS in individual vessel slices, which lends itself to more straightforward computation of these parameters, we developed a method of incorporating the whole 3D vascular surface for calculating surface area based WSS. It would be of interest to compare these two approaches in future studies to determine the relative benefits and weaknesses of each of these methods with respect to outcomes in patients with or at risk of developing AscAA. Using a surface approach, we are calculating WSS values over the entire vessel surface rather than sampling only a small fraction of the vessel wall, thus preventing sampling errors that may occur when trying to measure WSS values. Although it would be feasible using our method to analyze the WSS over the entire surface on a point-by-point basis, analysis of WSS in 12 areas, as reported in this study, simplifies group-wise comparisons and may be sufficient for larger, fusiform aneurysms.

An additional limitation of our study is the relatively small sample size, which may affect the statistical power of comparisons of peak WSS and time averaged WSS. In addition, the mean maximum diameter of the ascending aorta was 4.3cm, less than what is typically considered aneurismal. However, the mean z-score for maximum ascending aorta size was

6.12 and the aortic size index was also elevated. The fact that we were able to observe statistically significant differences in WSS between AscAD subjects and controls indicates that at even modest increases in ascending aorta size, we are able to observe measurable differences. In future longitudinal studies it will be important to study the effects of alterations in WSS and aneurysm growth, dissection or rupture, especially in light of the fact that in a study by R.R. Davies, et al, approximately 25% of aortic ruptures occurred in patients with aortic size indices less than the median of 2.5 cm/m^2 (26).

The use of a manual human-dependant vessel surface definition method causes intra- and inter-observer variability, because the estimation of WSS is highly dependent on the accuracy of the vessel wall definition. The amount of intra- and inter-observer variability we observed in our study is probably within acceptable limits for the time averaged and diastolic baseline WSS values. The fact that we had greater variability with the peak systolic WSS measurements is most likely related to the differences in vessel wall definition and the fact that the greatest differences in velocities relative to the vessel wall occur during diastole. Automation of vessel segmentation would be expected to improve observer variability. Another means of improving the vessel segmentation would be the use of steady-state free precession sequences which have a higher inherent blood to vessel wall contrast (40). Its implementation to radially undersampled phase contrast imaging, however, has not yet been accomplished.

The VENC in this study was 80 cm/s in the majority of subjects to preserve high velocity-to-noise ratios for vessel boundary definition. This resulted in aliasing in areas with high flow velocities in the center of the vessel. However, we did not observe any aliasing near the vessel wall and therefore would not affect our WSS calculations. A lower VENC was chosen for these cases to allow for increased sensitivity to low flow velocities near the vessel wall and more accurate localization of the vessel wall. Subjects scanned with higher VENCs showed sufficient velocity sensitivity near the vessel walls to define them. The influence of VENC on WSS calculations would be of interest for future investigations.

WSS is known to affect endothelial cell function (41). While it has been demonstrated that endothelial cells respond to changes in WSS, the extent to which that response plays a role in aneurysm progression or formation, if at all, has yet to be demonstrated. Longitudinal studies of WSS in patients at risk for aneurysm development should provide insight into this relationship.

In conclusion, we performed time resolved, 3D vessel surface segmentation of high spatial resolution, 4D flow PC MRI with radial undersampling which allowed us to investigate the WSS dynamics during the cardiac cycle over the entire ascending aortic wall. We found that AscAD are associated with alterations in WSS and that these alterations correspond to changes in flow patterns and velocities. AscAD had increased WSS during diastole, reduced pulsatility in WSS values over the cardiac cycle, and delayed onset of WSS in systole compared to individuals with normal aortic anatomy. Spatial patterns of WSS in AscAD were also different from those in normal subjects.

References

1. Elefteriades JA. Thoracic aortic aneurysm: reading the enemy's playbook. Current problems in cardiology. 2008; 33(5):203–277. [PubMed: 18439439]

2. Kirsch EW, Radu NC, Allaire E, Loisance DY. Pathobiology of idiopathic ascending aortic aneurysms. Asian cardiovascular & thoracic annals. 2006; 14(3):254–260. [PubMed: 16714709]

3. Davies RR, Goldstein LJ, Coady MA, et al. Yearly rupture or dissection rates for thoracic aortic aneurysms: simple prediction based on size. The Annals of Thoracic Surgery. 2002; 73(1):17–27. discussion 27-18. [PubMed: 11834007]

4. Hope TA, Markl M, Wigstrom L, Alley MT, Miller DC, Herfkens RJ. Comparison of flow patterns in ascending aortic aneurysms and volunteers using four-dimensional magnetic resonance velocity mapping. Journal of magnetic resonance imaging : JMRI. 2007; 26(6):1471–1479. [PubMed: 17968892]

5. Weigang E, Kari FA, Beyersdorf F, et al. Flow-sensitive four-dimensional magnetic resonance imaging: flow patterns in ascending aortic aneurysms. European journal of cardio-thoracic surgery : official journal of the European Association for Cardio-thoracic Surgery. 2008; 34(1):11–16. [PubMed: 18515137]

6. Cheng C, Tempel D, van Haperen R, et al. Atherosclerotic lesion size and vulnerability are determined by patterns of fluid shear stress. Circulation. 2006; 113(23):2744–2753. [PubMed: 16754802]

7. Malek AM, Alper SL, Izumo S. Hemodynamic shear stress and its role in atherosclerosis. JAMA : the journal of the American Medical Association. 1999; 282(21):2035–2042. [PubMed: 10591386]

8. Meng H, Wang Z, Hoi Y, et al. Complex hemodynamics at the apex of an arterial bifurcation induces vascular remodeling resembling cerebral aneurysm initiation. Stroke; a journal of cerebral circulation. 2007; 38(6):1924–1931.

9. Boussel L, Rayz V, McCulloch C, et al. Aneurysm growth occurs at region of low wall shear stress: patient-specific correlation of hemodynamics and growth in a longitudinal study. Stroke; a journal of cerebral circulation. 2008; 39(11):2997–3002.

10. Jin S, Oshinski J, Giddens DP. Effects of wall motion and compliance on flow patterns in the ascending aorta. Journal of Biomechanical Engineering. 2003; 125(3):347–354. [PubMed: 12929239]

11. Leuprecht A, Perktold K, Kozerke S, Boesiger P. Combined CFD and MRI study of blood flow in a human ascending aorta model. Biorheology. 2002; 39(3-4):425–429. [PubMed: 12122262]

12. Les AS, Shadden SC, Figueroa CA, et al. Quantification of hemodynamics in abdominal aortic aneurysms during rest and exercise using magnetic resonance imaging and computational fluid dynamics. Annals of Biomedical Engineering. 2010; 38(4):1288–1313. [PubMed: 20143263]

13. Papaharilaou Y, Ekaterinaris JA, Manousaki E, Katsamouris AN. A decoupled fluid structure approach for estimating wall stress in abdominal aortic aneurysms. Journal of Biomechanics. 2007; 40(2):367–377. [PubMed: 16500664]

14. Wolters BJ, Rutten MC, Schurink GW, Kose U, de Hart J, van de Vosse FN. A patient-specific computational model of fluid-structure interaction in abdominal aortic aneurysms. Medical engineering & physics. 2005; 27(10):871–883. [PubMed: 16157501]

15. Barker AJ, Lanning C, Shandas R. Quantification of Hemodynamic Wall Shear Stress in Patients with Bicuspid Aortic Valve Using Phase-Contrast MRI. Annals of Biomedical Engineering. 2009 Journal Article.

16. Boussel L, Rayz V, Martin A, et al. Phase-contrast magnetic resonance imaging measurements in intracranial aneurysms in vivo of flow patterns, velocity fields, and wall shear stress: comparison with computational fluid dynamics. Magnetic resonance in medicine : official journal of the Society of Magnetic Resonance in Medicine / Society of Magnetic Resonance in Medicine. 2009; 61(2):409–417. [PubMed: 19161132]

17. Frydrychowicz A, Arnold R, Hirtler D, et al. Multidirectional flow analysis by cardiovascular magnetic resonance in aneurysm development following repair of aortic coarctation. Journal of cardiovascular magnetic resonance : official journal of the Society for Cardiovascular Magnetic Resonance. 2008; 10(1):30. [PubMed: 18538035]

18. Frydrychowicz A, Berger A, Russe MF, et al. Time-resolved magnetic resonance angiography and flow-sensitive 4-dimensional magnetic resonance imaging at 3 Tesla for blood flow and wall shear stress analysis. The Journal of thoracic and cardiovascular surgery. 2008; 136(2):400–407. [PubMed: 18692649]

19. Frydrychowicz A, Stalder AF, Russe MF, et al. Three-dimensional analysis of segmental wall shear stress in the aorta by flow-sensitive four-dimensional-MRI. Journal of magnetic resonance imaging : JMRI. 2009; 30(1):77–84. [PubMed: 19557849]

20. Oyre S, Pedersen EM, Ringgaard S, Boesiger P, Paaske WP. In vivo wall shear stress measured by magnetic resonance velocity mapping in the normal human abdominal aorta. European journal of vascular and endovascular surgery : the official journal of the European Society for Vascular Surgery. 1997; 13(3):263–271. [PubMed: 9129599]

21. Stalder AF, Russe MF, Frydrychowicz A, Bock J, Hennig J, Markl M. Quantitative 2D and 3D phase contrast MRI: optimized analysis of blood flow and vessel wall parameters. Magnetic resonance in medicine : official journal of the Society of Magnetic Resonance in Medicine / Society of Magnetic Resonance in Medicine. 2008; 60(5):1218–1231. [PubMed: 18956416]

22. Wentzel JJ, Corti R, Fayad ZA, et al. Does shear stress modulate both plaque progression and regression in the thoracic aorta? Human study using serial magnetic resonance imaging. Journal of the American College of Cardiology. 2005; 45(6):846–854. [PubMed: 15766817]

23. Du J, Fain SB, Gu T, Grist TM, Mistretta CA. Noise reduction in MR angiography with nonlinear anisotropic filtering. Journal of magnetic resonance imaging : JMRI. 2004; 19(5):632–639. [PubMed: 15112314]

24. Gu T, Korosec FR, Block WF, et al. PC VIPR: a high-speed 3D phase-contrast method for flow quantification and high-resolution angiography. AJNRAmerican journal of neuroradiology. 2005; 26(4):743–749.

25. Gautier M, Detaint D, Fermanian C, et al. Nomograms for aortic root diameters in children using two-dimensional echocardiography. Am J Cardiol. 2010; 105(6):888–894. [PubMed: 20211339]

26. Davies RR, Gallo A, Coady MA, et al. Novel measurement of relative aortic size predicts rupture of thoracic aortic aneurysms. Ann Thorac Surg. 2006; 81(1):169–177. [PubMed: 16368358]

27. Wolak A, Gransar H, Thomson LE, et al. Aortic size assessment by noncontrast cardiac computed tomography: normal limits by age, gender, and body surface area. JACC Cardiovasc Imaging. 2008; 1(2):200–209. [PubMed: 19356429]

28. Johnson KM, Francois C, Lum D, et al. Rapid comprehensive evaluation of luminography and hemodynamic function with 3D radially undersampled phase contrast imaging MRI. Conf Proc IEEE Eng Med Biol Soc. 2009; 2009:4057–4060. [PubMed: 19964098]

29. Johnson KM, Lum DP, Turski PA, Block WF, Mistretta CA, Wieben O. Improved 3D phase contrast MRI with off-resonance corrected dual echo VIPR. Magn Reson Med. 2008; 60(6):1329–1336. [PubMed: 19025882]

30. Bock J, Frydrychowicz A, Stalder AF, et al. 4D phase contrast MRI at 3 T: effect of standard and blood-pool contrast agents on SNR, PC-MRA, and blood flow visualization. Magn Reson Med. 2010; 63(2):330–338. [PubMed: 20024953]

31. Du J, Carroll TJ, Wagner HJ, et al. Time-resolved, undersampled projection reconstruction imaging for high-resolution CE-MRA of the distal runoff vessels. Magn Reson Med. 2002; 48(3):516–522. [PubMed: 12210917]

32. Hope MD, Hope TA, Meadows AK, et al. Bicuspid aortic valve: four-dimensional MR evaluation of ascending aortic systolic flow patterns. Radiology. 2010; 255(1):53–61. [PubMed: 20308444]

33. Kilner PJ, Yang GZ, Mohiaddin RH, Firmin DN, Longmore DB. Helical and retrograde secondary flow patterns in the aortic arch studied by three-directional magnetic resonance velocity mapping. Circulation. 1993; 88(5 Pt 1):2235–2247. [PubMed: 8222118]

34. Markl M, Draney MT, Hope MD, et al. Time-resolved 3-dimensional velocity mapping in the thoracic aorta: visualization of 3-directional blood flow patterns in healthy volunteers and patients. Journal of computer assisted tomography. 2004; 28(4):459–468. [PubMed: 15232376]

35. Bogren HG, Mohiaddin RH, Yang GZ, Kilner PJ, Firmin DN. Magnetic resonance velocity vector mapping of blood flow in thoracic aortic aneurysms and grafts. The Journal of thoracic and cardiovascular surgery. 1995; 110(3):704–714. [PubMed: 7564437]

36. Liu X, Weale P, Reiter G, et al. Breathhold time-resolved three-directional MR velocity mapping of aortic flow in patients after aortic valve-sparing surgery. Journal of magnetic resonance imaging : JMRI. 2009; 29(3):569–575. [PubMed: 19243038]

37. Kvitting JP, Ebbers T, Wigstrom L, Engvall J, Olin CL, Bolger AF. Flow patterns in the aortic root and the aorta studied with time-resolved, 3-dimensional, phase-contrast magnetic resonance imaging: implications for aortic valve-sparing surgery. The Journal of thoracic and cardiovascular surgery. 2004; 127(6):1602–1607. [PubMed: 15173713]

38. Markl M, Draney MT, Miller DC, et al. Time-resolved three-dimensional magnetic resonance velocity mapping of aortic flow in healthy volunteers and patients after valve-sparing aortic root replacement. The Journal of thoracic and cardiovascular surgery. 2005; 130(2):456–463. [PubMed: 16077413]

39. Frydrychowicz A, Berger A, Stalder AF, et al. Initial results from diameter dependence of thoracic aortic hemodynamics acquired by 4D flow-sensitive MRI at 3T. 15

40. Santini F, Wetzel SG, Bock J, Markl M, Scheffler K. Time-resolved three-dimensional (3D) phase-contrast (PC) balanced steady-state free precession (bSSFP). Magnetic resonance in medicine : official journal of the Society of Magnetic Resonance in Medicine / Society of Magnetic Resonance in Medicine. 2009; 62(4):966–974. [PubMed: 19585606]

41. Davies PF. Flow-mediated endothelial mechanotransduction. Physiological Reviews. 1995; 75(3): 519–560. [PubMed: 7624393]
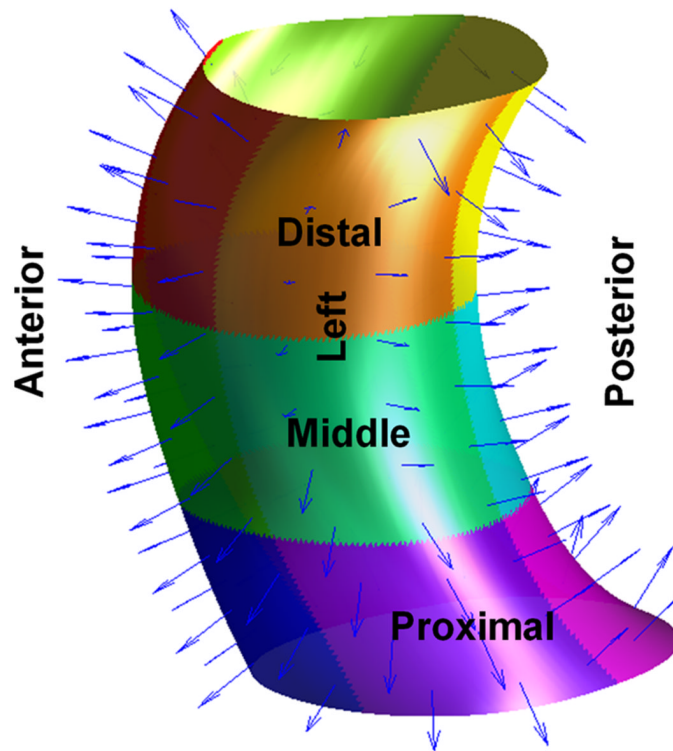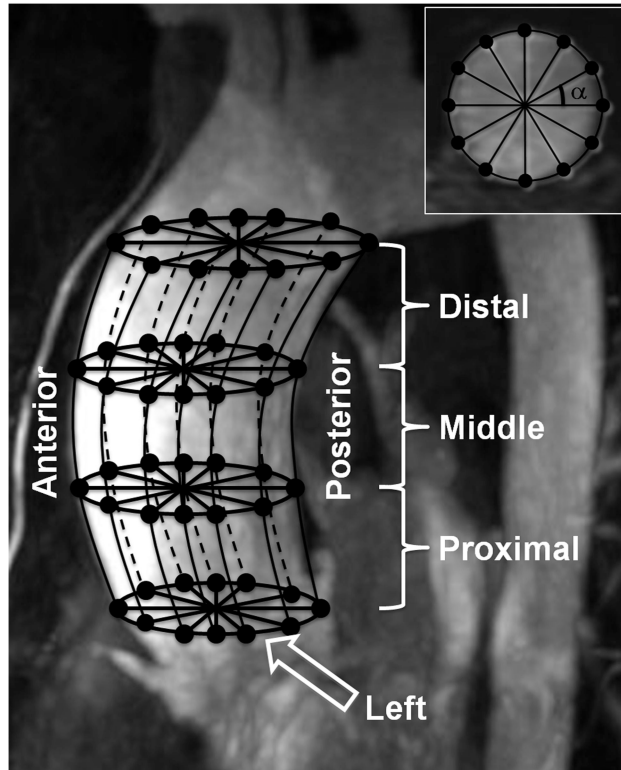
Figure 1.

Vessel surface definition, grid construction, and segmentation was based on complex difference angiograms. Vessel boundaries were manually segmented with an arbitrary number of reference points on axial cross-sectional slices (A, inset) from the aortic root to the bottom of the aortic arch. Subsequently anchor points were placed on the vessel contour, based on the angle, , around the centroid of the contour at that level. Vertical splines connected the anchor points between cross-sectional slices and were used for surface contour delineation. Interpolation of the vertical splines was used to form a 3D surface (B) and to calculate the surface normals (select samples are shown). The surface was divided into 12 segments (B, color-coded), three vertical (proximal, middle, and distal) and four circumferential (anterior, posterior, left, right).
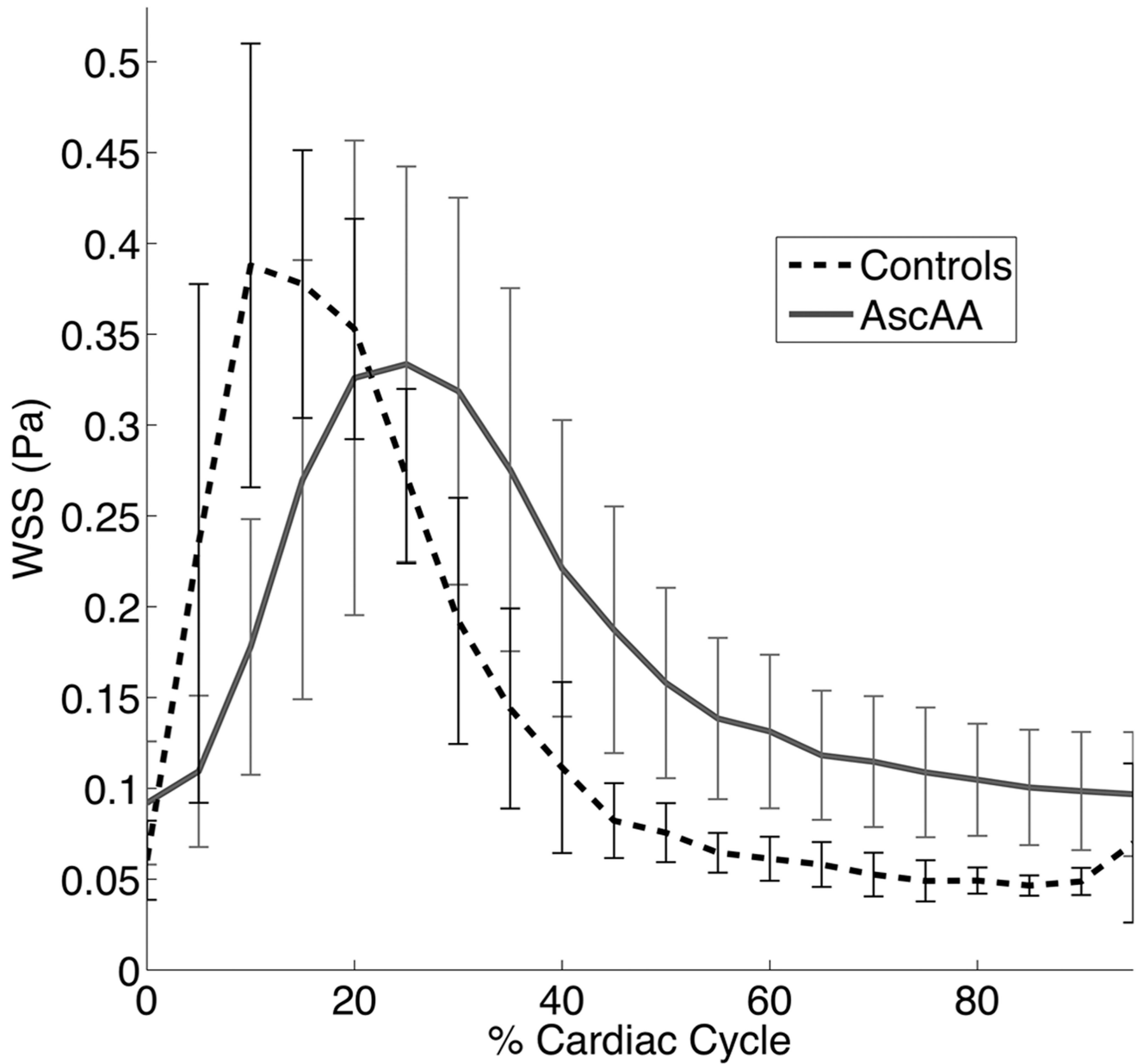
Figure 2.
Group averaged WSS magnitude for both AscAA and controls, averaged over the entire ascending aorta, is shown over one cardiac cycle. Error bars show the standard deviation. AscAA showed lower WSS during systole ($P = 0.17$), higher WSS in diastole ($P < 0.001$), and a later onset of peak WSS ($P < 0.001$).
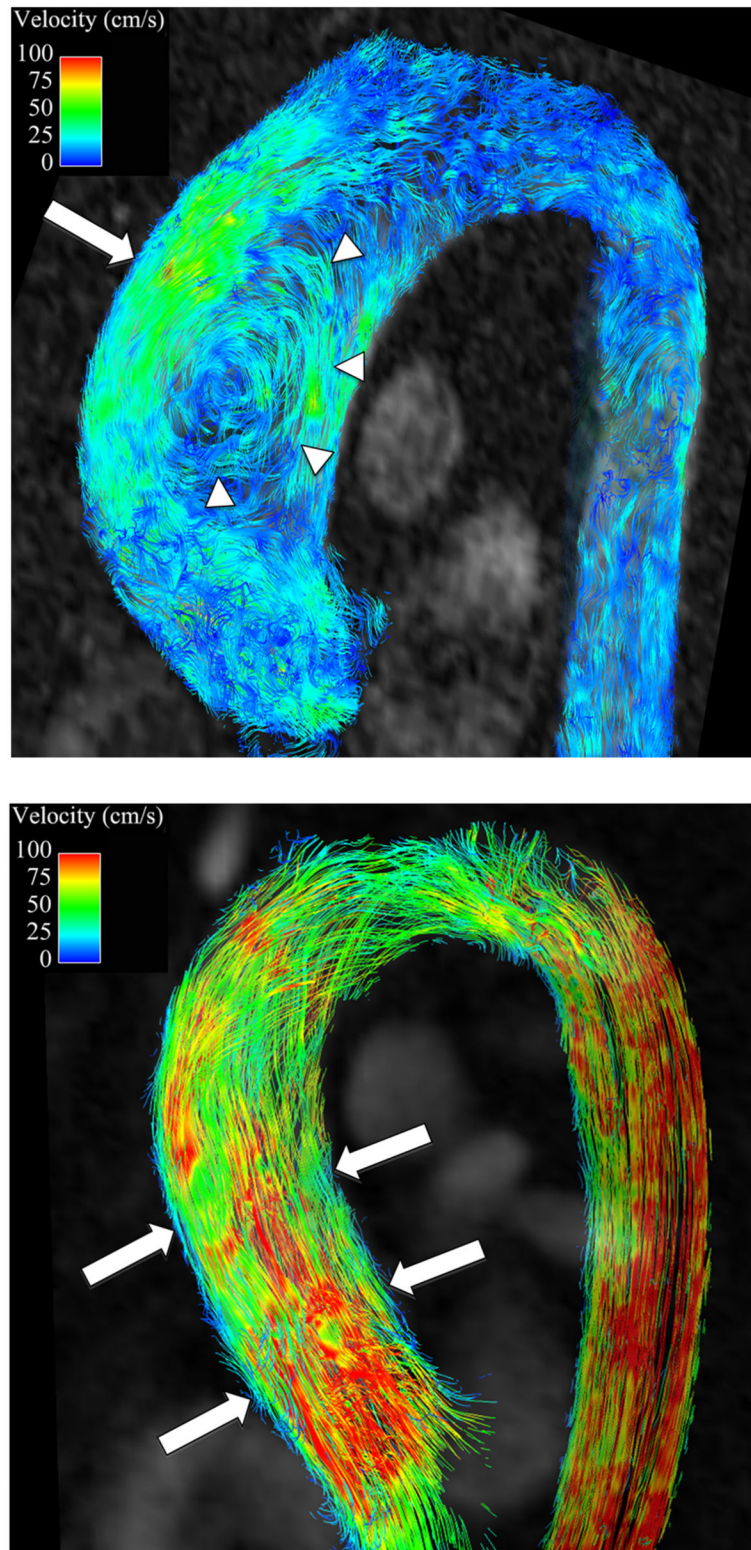
Figure 3.
Flow streamlines during peak systole in (A) a patient with an AscAA and (B) and normal healthy volunteer. In the patient with an AscAA (A), vortical flow (arrowheads) with higher

velocities are present along the anterior surface of the aneurysm (arrow), corresponding to areas of highest wall shear stress. In the healthy volunteer (B), flow is laminar (arrows). without vortices and with relatively uniform velocity distribution around the aorta surface, corresponding to observed uniform distribution of wall shear stress values.
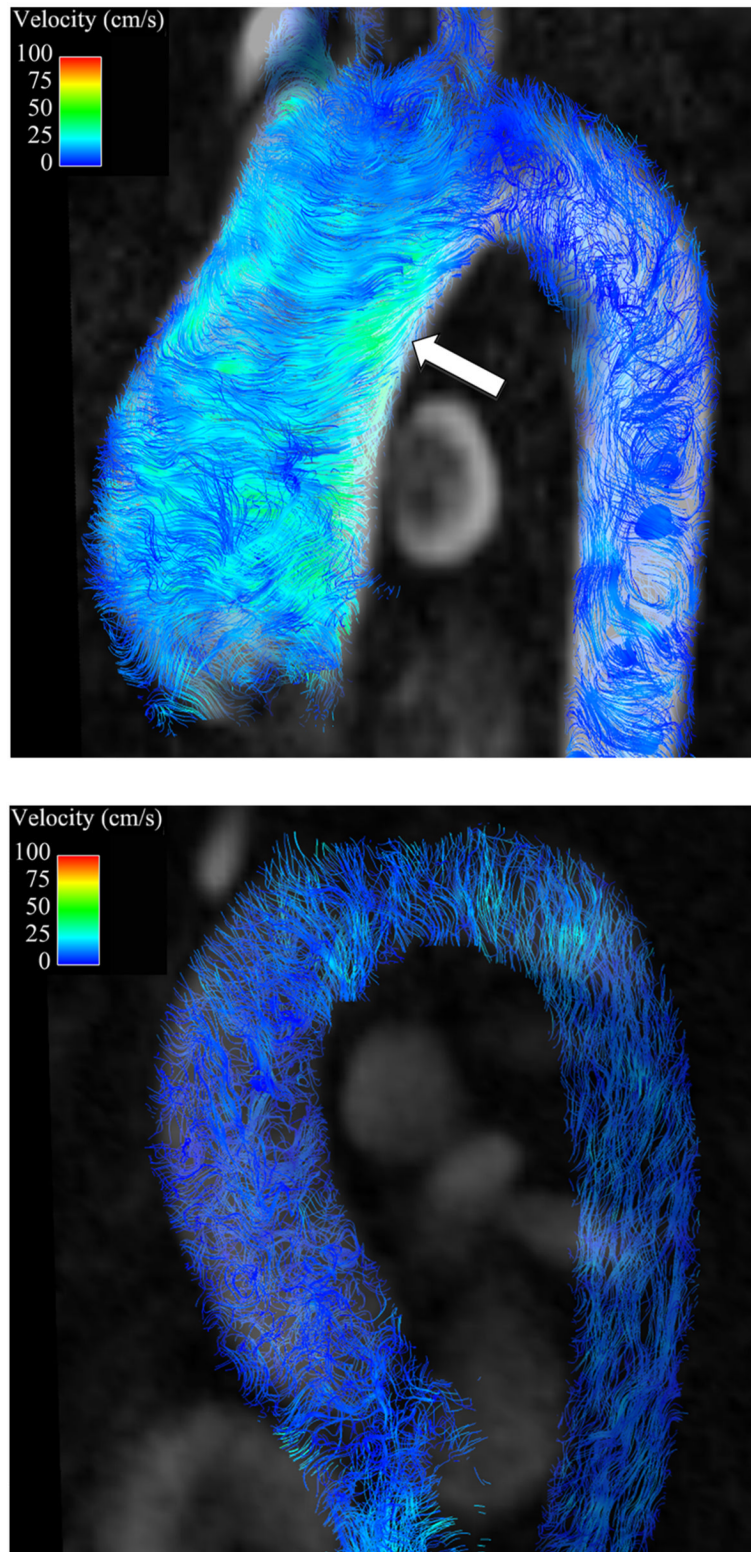
Figure 4.
Flow streamlines during diastole in (A) a patient with an AscAA and (B) and normal healthy volunteer. Helical flow (arrow) is present in the patient with AscAA (A) while in the normal

healthy volunteer (B), no helical pattern is observed. In addition, the velocities in the AscAA patient are higher than in the normal healthy volunteer, corresponding to the observation of higher diastolic wall shear stress values in AscAA patients than in normal healthy volunteers.

Table 1

WSS averaged over the cardiac cycle on each segment is reported in AscAD and controls. P (seg) denotes the resultant p-value of the paired student's t-test comparing WSS on each individual segment to the entire AscAD. P (group) denontes the resultant p-value from the unpaired student's t-test comparing AscAD to controls.

| Segment | Time averaged WSS | | | | | Peak Systolic WSS | | | | | Diastolic Baseline WSS | | | | |
| | AscAD | | Controls | | | AscAD | | Controls | | | AscAD | | Controls | | |
	WSS_{avg}	P (seg)	WSS'_{avg}	P (seg)	P (group)	WSS_s	P (seg)	WSS_s	P (seg)	P (group)	WSS_d	P (seg)	WSS_d	P (seg)	P (group)
Entire AscAo	0.17 ± 0.06		0.14 ± 0.01		0.07	0.35 ± 0.12		0.42 ± 0.09		0.17	0.10 ± 0.03		0.05 ± 0.01		<0.001
Anterior	0.20 ± 0.06	0.003	0.15 ± 0.03	0.1	0.02	0.51 ± 0.14	<0.001	0.46 ± 0.11	0.39	0.39	0.10 ± 0.03	0.93	0.05 ± 0.01	0.99	<0.001
Right	0.16 ± 0.06	0.042	0.15 ± 0.02	0.1	0.33	0.34 ± 0.15	0.49	0.48 ± 0.12	0.03	0.03	0.10 ± 0.04	0.06	0.05 ± 0.01	0.02	0.001
Posterior	0.16 ± 0.06	0.16	0.14 ± 0.02	0.43	0.18	0.30 ± 0.15	0.04	0.42 ± 0.14	0.07	0.07	0.11 ± 0.04	0.08	0.06 ± 0.01	0.02	<0.001
Left	0.17 ± 0.05	0.2	0.13 ± 0.01	<0.001	0.04	0.34 ± 0.14	0.46	0.40 ± 0.08	0.23	0.24	0.10 ± 0.03	0.52	0.05 ± 0.01	0.93	<0.001
Distal	0.17 ± 0.06	0.87	0.15 ± 0.02	0.006	0.16	0.37 ± 0.15	0.42	0.47 ± 0.12	0.1	0.1	0.10 ± 0.03	0.78	0.06 ± 0.01	0.004	<0.001
Middle	0.18 ± 0.06	<0.001	0.14 ± 0.02	0.32	0.03	0.39 ± 0.12	<0.001	0.44 ± 0.10	0.33	0.33	0.10 ± 0.03	0.07	0.05 ± 0.01	0.02	<0.001
Proximal	0.16 ± 0.05	0.01	0.13 ± 0.01	0.03	0.09	0.35 ± 0.11	0.57	0.39 ± 0.09	0.3	0.3	0.10 ± 0.04	0.54	0.05 ± 0.01	0.14	<0.001
Distal Anterior	0.19 ± 0.07	0.053	0.15 ± 0.03	0.12	0.05	0.54 ± 0.22	0.001	0.49 ± 0.12	0.042	0.55	0.09 ± 0.03	0.28	0.05 ± 0.01	0.029	<0.001
Distal Right	0.15 ± 0.06	0.043	0.16 ± 0.02	0.009	0.93	0.32 ± 0.16	0.13	0.54 ± 0.15	0.004	0.004	0.10 ± 0.04	0.34	0.06 ± 0.01	0.19	0.003
Distal Posterior	0.16 ± 0.07	0.29	0.14 ± 0.02	0.77	0.23	0.34 ± 0.18	0.77	0.45 ± 0.13	0.16	0.14	0.11 ± 0.04	0.15	0.06 ± 0.01	<0.001	0.001
Distal Left	0.17 ± 0.05	0.7	0.14 ± 0.01	0.21	0.09	0.38 ± 0.14	0.19	0.47 ± 0.11	0.13	0.13	0.11 ± 0.03	0.26	0.06 ± 0.01	0.031	<0.001
Middle Anterior	0.21 ± 0.05	<0.001	0.15 ± 0.03	0.21	0.007	0.57 ± 0.12	<0.001	0.47 ± 0.13	0.25	0.09	0.10 ± 0.03	0.67	0.05 ± 0.01	0.36	<0.001
Middle Right	0.17 ± 0.06	0.84	0.15 ± 0.03	0.061	0.26	0.39 ± 0.19	0.24	0.52 ± 0.12	0.003	0.08	0.09 ± 0.04	0.13	0.05 ± 0.01	0.006	<0.001
Middle Posterior	0.18 ± 0.06	0.48	0.14 ± 0.02	0.8	0.07	0.37 ± 0.15	0.71	0.46 ± 0.15	0.16	0.16	0.11 ± 0.03	0.026	0.05 ± 0.01	0.4	<0.001
Middle Left	0.16 ± 0.06	0.77	0.13 ± 0.02	0.002	0.03	0.39 ± 0.16	0.29	0.44 ± 0.10	0.65	0.42	0.11 ± 0.04	0.086	0.05 ± 0.01	0.15	<0.001
Proximal Anterior	0.18 ± 0.05	0.23	0.15 ± 0.02	0.039	0.06	0.47 ± 0.12	0.018	0.48 ± 0.11	0.058	0.96	0.11 ± 0.04	0.072	0.06 ± 0.01	0.34	<0.001
Proximal Right	0.16 ± 0.06	0.015	0.13 ± 0.02	0.013	0.09	0.38 ± 0.15	0.27	0.43 ± 0.12	0.68	0.35	0.09 ± 0.04	0.015	0.05 ± 0.01	<0.001	<0.001
Proximal Posterior	0.16 ± 0.06	0.006	0.13 ± 0.03	0.45	0.33	0.31 ± 0.16	0.05	0.43 ± 0.19	0.84	0.11	0.10 ± 0.04	0.98	0.05 ± 0.01	0.16	0.001
Proximal Left	0.15 ± 0.05	0.01	0.11 ± 0.02	<0.001	0.04	0.35 ± 0.12	0.16	0.35 ± 0.10	0.025	0.48	0.10 ± 0.03	0.24	0.05 ± 0.01	0.4	0.001

Table 2

Intra- and inter-observer variability for time-averaged, peak systolic and diastolic baseline WSS measurements. Values reported are mean ± standard deviation percent differences in WSS values over the entire ascending aorta. The intra- and inter-observer variability are less than the differences in mean values for WSS values between patients with AscAD and controls.

	Time averaged WSS		Peak Systolic WSS		Diastolic Baseline WSS	
	AscAD	Controls	AscAD	Controls	AscAD	Controls
Intra-observer Variability	1.16 ± 0.15 %	1.58 ± 2.01 %	5.29 ± 2.02 %	6.40 ± 7.94 %	1.50 ± 0.36 %	0.74 ± 0.88 %
Inter-observer Variability	3.69 ± 4.65 %	7.48 ± 6.47 %	13.26 ± 12.43 %	14.71 ± 12.57 %	8.66 ± 4.74 %	2.84 ± 1.60 %
% Difference of means	19.35%		18.18%		66.67 %	